decide on the eventual behavior of the network. The network was considered to have settled into a fixed point when the total activity on two consecutive iterations differed by less than the settling threshold ϵ, which was set to the value 0.001 in all these experiments. An upper bound, B, determined when the network failed to settle. Computation was stopped when the total activity in the network either settled or reached this bound. In practice, we used relatively small networks and values of B, thus limiting the number of iterations. Since limiting the total number of iterations smoothes the expected transition we varied B in order to examine its effect.

The results of the first two experiments are depicted in Fig. 2. They explore left-to-right movement on the phase diagram as the value of μ increases. This path corresponds to the trajectory labeled 1&2 in Fig. 1. For both of these experiments $\alpha = 0.6$ and $\gamma = 0.4$, so $\alpha/\gamma = 1.5$. In experiment 1 (solid curve), $B = 10$ and in experiment 2 (dashed curve), $B = 1000$. Figure 2A shows the extent of the spatial event horizon by displaying the average fraction (over the 25 trials) of active nodes in the network at the time the network either settles or reaches the value B. As expected from the limited size of our network, the transition is smoothed out. To highlight the transition, we examined the relative fluctuations in the network, computed by dividing the standard deviation of the fraction of active nodes by their average. This quantity, shown in Fig. 2B, peaks at approximately the predicted point of 50 links ($\mu = 1$).

The results depicted in Fig. 3 are from the remaining two experiments. We investigated movement in the vertical direction on the phase diagram, as shown by transitions 3 and 4 of Fig. 1. In both of these cases, α and γ begin at 0.4 and 0.6, respectively; α is increased by 0.02 while γ is decreased by the same amount, until their ratio reaches the value 1.5. The vertical transition was tried at two different values of μ, 0.4 and 1.4, corresponding to 20 links (solid curve) and 70 links (dashed curve). Figure 3A shows the total activity of the network when the network either settles or reaches the bound $B = 100.0$. One can clearly see the predicted sudden growth in activity when $\alpha/\gamma = 1.0$. Below this point the network always settles. Above it, the activity continues to grow and eventually reaches B. The difference in the upper part of these curves (about 30 for the solid curve and about 75 for the dashed curve) is a result of the overall greater number of connected nodes in the latter case.

Figure 3B shows the time taken for the network to either settle or reach the value B. In this figure we have separated each curve into the settling region (left) and bounded region (right). The peak is a result of different phenomena on either side. On the left, the curve results from the time required for the network to settle to its fixed point, whereas on the right instead of settling the network continues to grow faster as α/γ increases, reaching the value B more rapidly.

The theory developed by Huberman and Hogg (*8*) provides a way of understanding the robust global features of a system. Such features, which are hard to notice in small systems, can play a large role in the behavior of larger ones. Our results clearly show that the predicted phase transitions can be observed even in relatively small spreading activation networks. Moreover, the existence of such transitions has immediate implications for the predictions of memory models and the behavior of artificial intelligence systems which incorporate learning. Specifically, instead of the fairly smooth transitions in performance that have been generally assumed in these situations, we have shown that abrupt transitions can be expected. More generally, these experiments show that statistical models provide a useful way to understand the behavior of large systems. They also emphasize the dominating influence of topological properties. These are particularly important implications for the behavior of any network with a dynamic topology.

REFERENCES AND NOTES

1. See J. R. Anderson [*The Architecture of Cognition* (Harvard Univ. Press, Cambridge, MA, 1983)] for a discussion and analysis of spreading activation. Also see J. R. Anderson and G. H. Bower [*Human Associative Memory* (Lawrence Earlbaum, Hillsdale, NJ, 1979)] for a brief review of its history.
2. M. R. Quillian, in *Semantic Information Processing*, M. Minsky, Ed. (MIT Press, Cambridge, MA, 1968). Spreading activation is used to compare and contrast word-senses in a network-structured dictionary database.
3. A. Howe, in *Proceedings of the Canadian Society for Computational Studies of Intelligence* (London, Ontario, 1984), pp. 25–27.
4. P. R. Cohen and P. M. Stanhope, in *Proceedings of the 6th International Workshop on Expert Systems and their Applications*, Avignon, France, 28–30 April 1986. Spreading activation is used to find suggested granting agencies to which proposals can be sent.
5. A. M. Collins and E. F. Loftus, *Psychol. Rev.* **82**, 407 (1975).
6. D. Lenat, M. Prakash, M. Shepard, *Artif. Intell. Mag.* **6**, 65 (Winter 1986).
7. D. Hillis, *The Connection Machine: Computing for the New Wave* (MIT Press, Cambridge, MA, 1986).
8. B. A. Huberman and T. Hogg, *Artif. Intell.*, in press.
9. G. Deutscher, R. Zallen J. Adler, Eds., *Percolation Structures and Processes, Annals of the Israeli Physical Society* (Hilger, Bristol, 1983), vol. 5.

10. We have benefited from discussions with A. Howe.

27 October 1986; accepted 10 April 1987

Single-Channel and Genetic Analyses Reveal Two Distinct A-Type Potassium Channels in *Drosophila*

CHARLES K. SOLC, WILLIAM N. ZAGOTTA, RICHARD W. ALDRICH*

Whole-cell and single-channel voltage-clamp techniques were used to identify and characterize the channels underlying the fast transient potassium current (A current) in cultured myotubes and neurons of *Drosophila*. The myotube (A_1) and neuronal (A_2) channels are distinct, differing in conductance, voltage dependence, and gating kinetics. The myotube currents have a faster and more voltage-dependent macroscopic inactivation rate, a larger steady-state component, and a less negative steady-state inactivation curve than the neuronal currents. The myotube channels have a conductance of 12 to 16 picosiemens, whereas the neuronal channels have a conductance of 5 to 8 picosiemens. In addition, the myotube channel is affected by *Shaker* mutations, whereas the neuronal channel is not. Together, these data suggest that the two channels are separate molecular structures, the expression of which is controlled, at least in part, by different genes.

THE OPPORTUNITY TO COMBINE genetic, molecular, and single-channel analyses makes *Drosophila* an ideal preparation for the study of ion-channel function. By analyzing the effects of genetic mutations on the gating behavior of single ion channels, the influence of small changes in structure on channel function can be examined. A number of behavioral mutations proposed to affect ion channels have been isolated (*1–3*). Mutations at the *Shaker* locus alter or eliminate A-type potassium currents in larval and adult muscle cells, suggesting that the mutation lies in a structural gene for the A-current channel (*4–7*). *Shaker* mutations also cause hyperexcitability of larval presynaptic terminals (*8, 9*) and abnormally long action potentials in the adult giant axon (*10*), effects that are mim-

Department of Neurobiology, Stanford University Medical School, Stanford, CA 94305.

*To whom correspondence should be addressed.

icked by the application of 4-aminopyridine (4-AP) to wild-type preparations (*8, 10*). These results lead to the suggestion that the A current is decreased in neurons from *Shaker* flies (*4*). We have now characterized single K^+ channels underlying A currents in both cultured myotubes and neurons and demonstrated that there are at least two classes of A channels, one that is affected by *Shaker* mutations and one that is not.

We were able to study the A currents in both cell types in relative isolation. A large fraction of the myotubes that had been in culture for 10 to 14 hours and a subpopulation of the neurons (regardless of culture age) expressed primarily A currents. The myotube and neuronal A currents differed in the voltage dependence of both their kinetic and steady-state properties. Whole-cell currents under voltage clamp from a Canton-S wild-type myotube and neuron are shown in Fig. 1A. The time courses of both macroscopic activation and inactivation of the myotube current were voltage dependent. The current turned on slowly at low voltages. As the voltage was increased, it turned on faster and developed a larger and more rapidly inactivating component that decayed to a steady-state value. These myotube currents are similar in both voltage dependence and kinetics to the A currents recorded in adult muscle (*11*) at a similar temperature (20° to 23°C) and were similarly blocked by 5 m*M* external 4-AP. The neuronal A current behaved differently. The macroscopic activation rate was voltage-dependent only at the lowest voltages, and the macroscopic inactivation rate was largely independent of voltage over the entire range studied. The neuronal current inactivated completely with a double-exponential time course that was slower than the rate of decay seen in myotube A current (note the difference in time scales in Fig. 1). The two currents also differed in their voltage dependence of activation and inactivation. The myotube current began to turn on at more positive voltages (Fig. 1C) and had a less negative prepulse inactivation curve (Fig. 1D) than the neuronal current. The myotube current (Fig. 1B1) showed no reduction in amplitude after a prepulse to −50 mV, a prepulse voltage that almost completely inactivated the neuronal current (Fig. 1B2). The slopes of the Boltzmann distributions fitted to the prepulse inactivation data (Fig. 1D) are similar (*e*-fold for 6.4 mV), but the midpoint of inactivation for the neuronal current (−75 mV; range, −95 to −75 mV) is more negative than the midpoint of inactivation for the myotube current (−30 mV; range, −35 to −25 mV).

We also saw differences in the two currents at the single-channel level, confirming that the whole-cell measurements reflect differences in the channels themselves and are not due to different complications in neurons and myotubes such as space clamp, series-resistance error, current separation, or ion accumulation. Representative traces and ensemble averages of single A-current channels recorded at different voltages in outside-out patches from a myotube and a neuron are shown in Fig. 2. Because the currents were recorded in the presence of 10 n*M* internal free Ca^{2+} buffered with 11 m*M* EGTA, it is improbable that either channel corresponds to the transient Ca^{2+}-activated K^+ channel in adult and larval muscle (*12, 13*). Both of these channels can be identified as A-type channels because of their rapid rate of decay and negative prepulse inactiva-

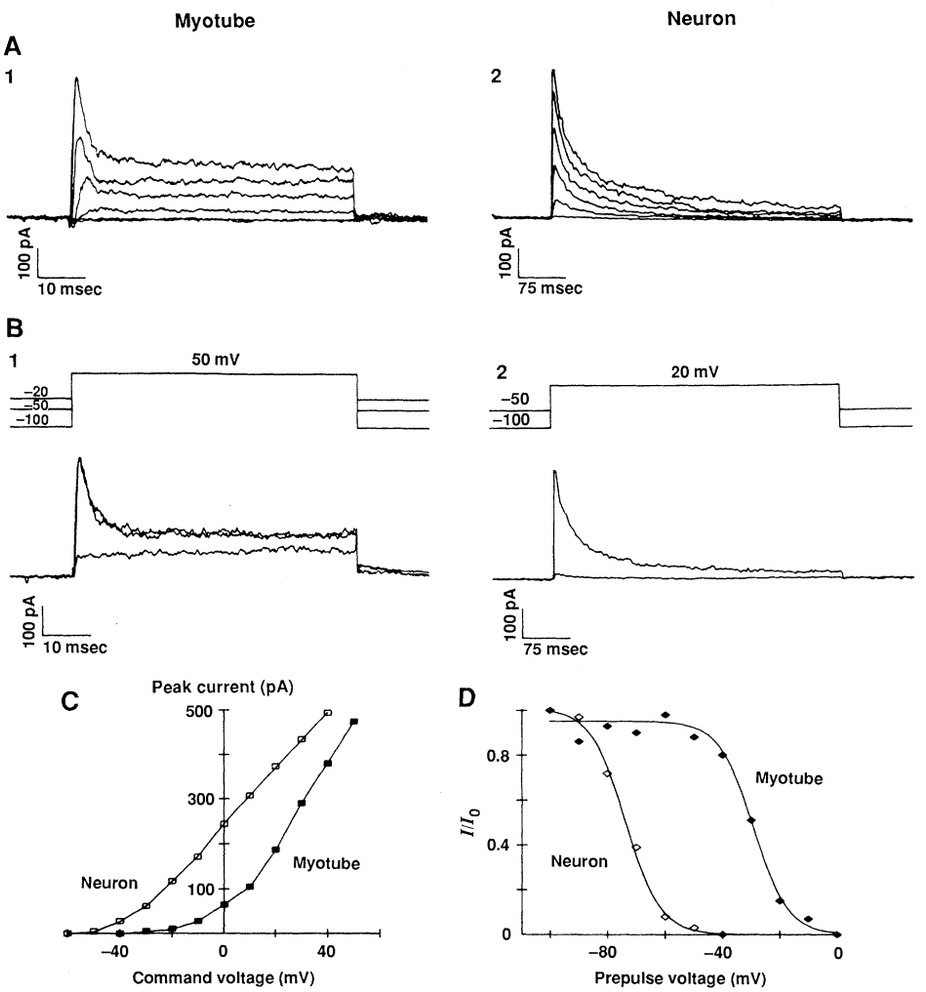

Fig. 1. Whole-cell transient potassium currents recorded from cultured *Drosophila* embryonic myotubes and larval central nervous system neurons. (**A**) A currents recorded from an embryonic myotube (A1) and a larval neuron (A2) of *Drosophila*. The membrane voltage was held at a prepulse potential (V_P) of −100 mV for 500 msec (1) or 300 msec (2) and successively depolarized to command potentials (V_C) between −50 and 50 mV in 20-mV steps. Pulse duration was 80 msec (1) or 450 msec (2). (**B**) A currents evoked by steps to 50 mV (1) or 20 mV (2) from prepulse potentials of −100, −50, and −20 mV (1) or −100 and −50 mV (2). (**C**) Peak current plotted as a function of voltage for the myotube and neuronal A-current families in (A). (**D**) Prepulse inactivation curves for the myotube and neuronal currents in (B). Normalized peak currents minus noninactivating currents are plotted as a function of the prepulse voltage, and the data are fitted with Boltzmann distributions (I, current; I_o, current after −100 mV prepulse; see text for parameters). The myotubes differentiate in cell cultures made by the single-embryo protocol developed by Seecof (*20*). The cultures were incubated at 26°C for 10 to 14 hours before recording. Neuronal cultures were prepared from the brain hemispheres and ventral ganglia of late third instar larvae by a method similar to that described by Wu *et al.* (*21*). The cultures were incubated at 22°C for 3 to 6 days before use. We used standard whole-cell and single-channel recording methods (*22*). The experiments were conducted at room temperature (20° to 23°C). The solution used in the pipette was 70 m*M* KF, 70 m*M* KCl, 2 m*M* $MgCl_2$, 11 m*M* EGTA, 1 m*M* $CaCl_2$ (10 n*M* free Ca^{2+}), 10 m*M* Hepes (KOH), *p*H 7.2 and in the bath 140 m*M* NaCl, 2 m*M* KCl, 4 m*M* $MgCl_2$, 2 m*M* $CaCl_2$, 5 m*M* Hepes (NaOH), *p*H 7.1. The free Ca^{2+} concentration in the pipette was buffered at 10 n*M* with 11 m*M* EGTA. Linear leakage and uncompensated capacitive currents were subtracted on-line. Current records were filtered at 2 kHz with an eight-pole Bessel filter and digitized at 0.1 msec per point (myotube) or 3 msec per point (neuron).

tion curves (*14–16*). Therefore, we designate these channels as A_1 (myotube) and A_2 (neuron). We have never seen the A_1 channel in neurons or the A_2 channel in myotubes, but it is possible that either channel may be found in the other tissue under different experimental conditions, at different developmental stages, or in other regions of the cell membranes. The kinetics and voltage dependence of the ensemble averages of both channels closely resembled those of the whole-cell A currents shown in Fig. 1A. The A_1 channel averages turned on slowly at low voltages but became faster and more transient at higher voltages, whereas the A_2-channel averages were transient over the entire voltage range. The A_2-channel ensemble averages inactivated along a double-exponential time course that is quantitatively similar to the neuronal whole-cell currents. The steady-state component apparent in the A_1-channel ensemble averages suggests that some of the steady-state current in the myotube whole-cell records (Fig. 1A) can be attributed to the A_1 channels. The steady-state inactivation of the two channels also agrees with the whole-cell A currents in the two cell types. Figure 3A shows that the A_1 channels are not inactivated after a prepulse to −50 mV but are inactivated after a prepulse of −20 mV, whereas the A_2 channels (Fig. 3B) are completely inactivated after a prepulse to −80 mV. The midpoint of inactivation for the A_2 channels shown in this figure is more negative than the midpoint of inactivation for the whole-cell currents shown in Fig. 1, but falls within the range found for the neuronal A channels. Taken together these results strongly suggest that the A_1 and A_2 channels underlie the whole-cell A currents in myotubes and neurons, respectively.

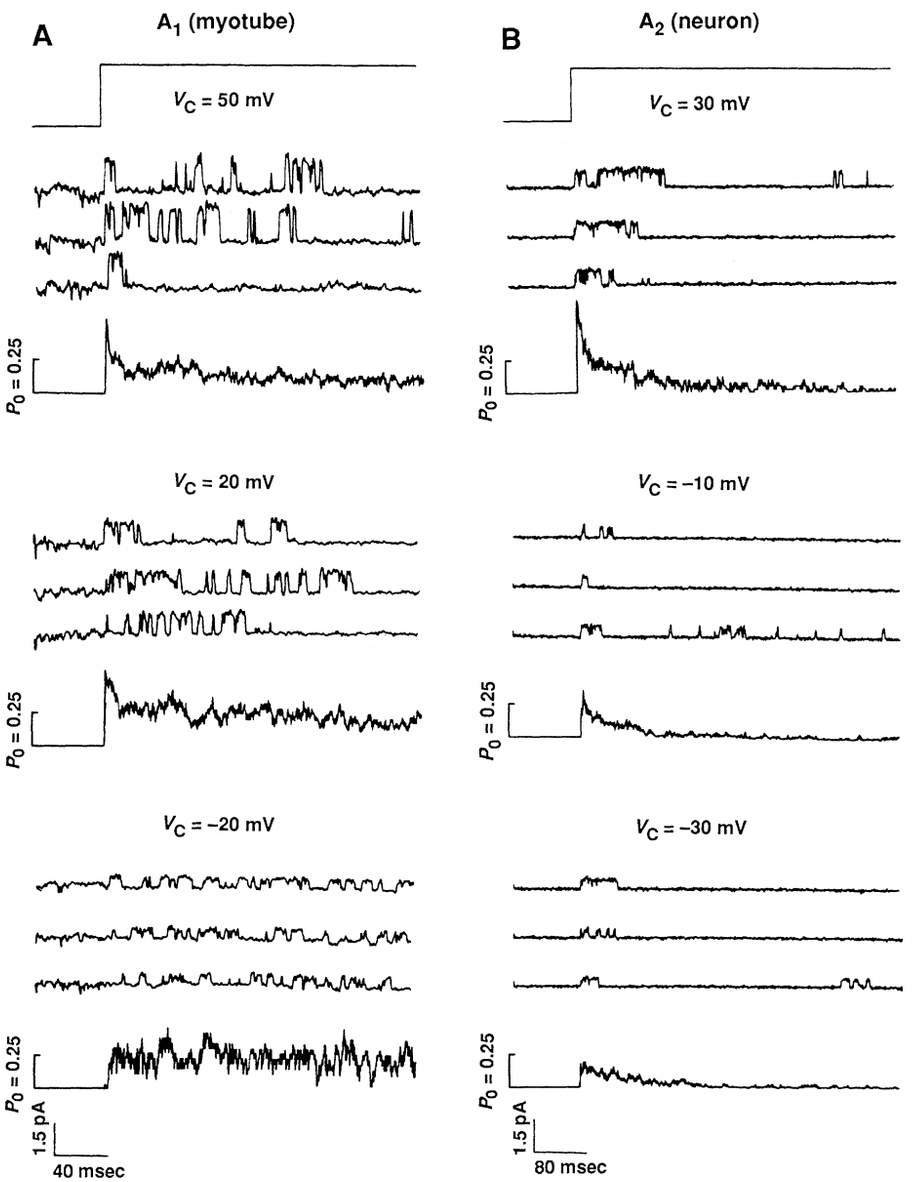

Fig. 2. Single A channels recorded in outside-out patches from a myotube (**A**) and a neuron (**B**). The membrane was held at a negative prepulse potential (−100 to −120 mV) for 500 msec and then stepped to V_C for 240 msec (myotube) or 480 msec (neuron). Each panel shows three representative sweeps generated by steps to the command potential shown and an ensemble average of many such sweeps at the same potential. The ensemble averages are plotted as probability of the channel being open (P_0). They can be compared to whole-cell records in Fig. 4A (myotube) and Fig. 1A2 (neuron) at a similar time scale. Vertical scale bar is 1.5 pA for the single traces and P_0 = 0.25 for the ensemble averages. Experimental conditions were the same as in Fig. 1. The data were filtered at 1 kHz and digitized at 100 μsec per point (myotube) and 400 μsec per point (neuron). Leak and uncompensated capacitance currents were digitally subtracted by using leak templates constructed by fitting smooth functions to sweeps with no openings. The records were then idealized with a 50% criterion method (*23*), and ensemble averages were generated from the idealized data. The single-channel records shown were digitally filtered at 500 Hz for display purposes.

Because of previous reports of alterations in A current in larval and adult muscle and hyperexcitable presynaptic terminals in *Shaker* flies, we have examined the effect of *Shaker* mutations on the A_1 and A_2 channels. The A_1 channel currents are eliminated in myotubes carrying *Shaker* null alleles (n = 12), whereas the A_2 channel is not measurably affected by *Shaker* mutations. Figure 4 (top) shows whole-cell myotube current families from wild-type flies and from mutants homozygous for Sh^{KS133}, an allele that has been shown to eliminate A current in larval and adult muscle (*4, 9, 17*). The myotube A current is absent in cells homozygous for either Sh^{KS133} or Sh^{P}, another *Shaker* null allele. The bottom panel shows single A_2 channel currents and ensemble averages in wild type and Sh^{KS133}. We found no detectable difference between the A_2 channels in wild type and Sh^{KS133} or Sh^{5}, an

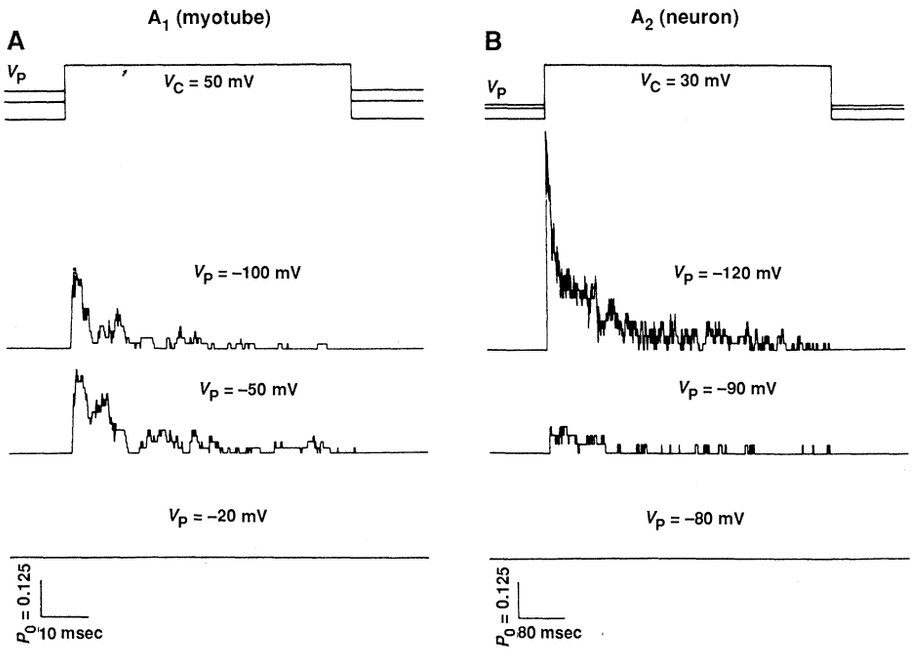

Fig. 3. Prepulse inactivation of A_1 channels (**A**) and A_2 channels (**B**). Ensemble averages from idealized single-channel data recorded during steps from three different prepulse potentials. The A_1 channel is completely inactivated with a 500-msec prepulse to −20 mV (no openings in 12 sweeps, at least one channel in the patch), and the A_2 channel is completely inactivated with a 500-msec prepulse to −80 mV (no openings in 16 sweeps, at least two channels in the patch). In each case, the data for the averages with no openings were obtained between runs from more negative prepulse potentials to control for possible run down of the currents.

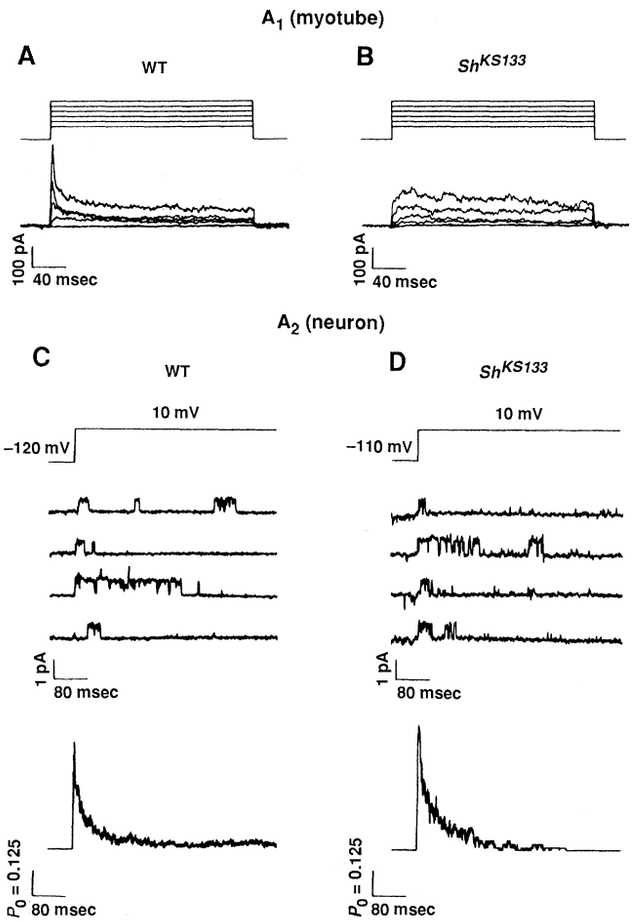

Fig. 4. Effect of *Shaker* mutations on the A_1 and A_2 channels. Whole-cell currents from myotubes (**A** and **B**) and single-channel currents with ensemble averages from neurons (**C** and **D**) in wild-type (WT in A and C) and Sh^{KS133} (B and D) cells. The whole-cell current families were generated as in Fig. 1, filtered at 2 kHz, and sampled at 400 μsec per point. V_P was −100 mV and V_C was stepped incrementally between −50 and 50 mV in 20-mV steps in both sets of records. Single-channel data were recorded, analyzed, and displayed as in Fig. 2. The A_1 current seen in wild-type myotubes (A) is eliminated in cells from animals homozygous for the Sh^{KS133} mutations (B). The A_2 channel, on the other hand, is present and not significantly altered in cells homozygous for the Sh^{KS133} mutation (C and D).

allele that changes the voltage dependence and kinetics of the A current in larval and adult muscle (*4, 7*), with respect to single-channel current, voltage dependence, or kinetics.

Although we have found no effect of Sh^{KS133} and Sh^{5} on the A_2 channels, these mutations can have a profound effect on neuronal excitability (*8–10*). There are several possible explanations for this seeming discrepancy. (i) The A_1 channel may be expressed in the soma of only a small population of neurons from which we did not record currents. (ii) The A_1 channels may be present only in the processes of the neurons and therefore do not show up in whole-cell currents and patches. (iii) The *Shaker* gene product may affect an outward current channel different from A_1 in the neurons. Our results do not distinguish between these possibilities, but suggest that there is a locus in addition to *Shaker* that codes for fast transient voltage-dependent K^+ channels in *Drosophila*.

Recently, single A-current channels have been described in mammalian sensory neurons (*18, 19*). Their conductances are approximately 20 pS, and inactivation time constants are in the range of 30 and 100 msec. Neither the A_1 nor the A_2 channels closely resemble the mammalian A channels, as the A_2 channel has a substantially smaller conductance (5 to 8 pS), and the A_1 channel has a similar conductance but a considerably faster inactivation time course. We have, however, characterized a class of 14- to 24-pS channels in both neurons and myotubes that inactivate more slowly than the A_1 and A_2 channels, with a time course more similar to the mammalian A channels. We also have characterized several noninactivating channels in both preparations. The characterization of each of these channel types provides the groundwork for determining the alterations in gating that result from structural changes in the channels from mutant flies.

REFERENCES AND NOTES

1. J. C. Hall, *Q. Rev. Biophys.* **15**, 223 (1982).
2. B. Ganetzky and C.-F. Wu, *Trends Neurosci.* **8**, 322 (1985).
3. L. Salkoff and M. A. Tanouye, *Physiol. Rev.* **66**, 301 (1986).
4. L. Salkoff and R. Wyman, *Nature (London)* **293**, 228 (1981).
5. L. Salkoff, *Cold Spring Harbor Symp. Quant. Biol.* **48**, 221 (1983).
6. C.-F. Wu, B. Ganetzky, F. N. Haugland, A.-X. Liu, *Science* **220**, 1076 (1983).
7. C.-F. Wu and F. N. Haugland, *J. Neurosci.* **10**, 2626 (1985).
8. Y. N. Jan, L. Y. Jan, M. J. Dennis, *Proc. R. Soc. London Ser. B* **198**, 87 (1977).
9. B. Ganetzky and C.-F. Wu, *J. Neurogenet.* **1**, 17 (1983).
10. M. A. Tanouye, A. Ferrus, S. C. Fujita, *Proc. Natl. Acad. Sci. U.S.A.* **78**, 6548 (1981).
11. L. Salkoff and R. J. Wyman, *ibid.* **77**, 6216 (1980).
12. L. Salkoff, *Nature (London)* **302**, 249 (1983).

13. S. Singh, C.-F. Wu, B. Ganetzky, *Soc. Neurosci. Abstr.* **12**, 559 (1986).
14. S. H. Thompson and R. W. Aldrich, *Cell Surf. Rev.* **6**, 49 (1980).
15. D. J. Adams, S. J. Smith, S. H. Thompson, *Annu. Rev. Neurosci.* **3**, 141 (1980).
16. M. A. Rogawski, *Trends Neurosci.* **8**, 214 (1985).
17. L. C. Timpe and L. Y. Jan, *J. Neurosci.*, in press.
18. E. Cooper and A. Shrier, *J. Physiol. (London)* **369**, 199 (1984).
19. H. Kasai, M. Kameyama, K. Yamaguchi, J. Fukuda, *Biophys. J.* **49**, 1243 (1986).
20. R. L. Seecof, *TCA Manual* **5**, 1019 (1979).
21. C.-F. Wu, N. Suzuki, M.-M. Poo, *J. Neurosci.* **3**, 1888 (1983).
22. O. P. Hamill, A. Marty, E. Neher, B. Sakmann, F. J. Sigworth, *Pfluegers Arch.* **391**, 85 (1981).
23. D. Colquhoun and F. J. Sigworth, in *Single-Channel Recording*, B. Sakmann and E. Neher, Eds. (Plenum, New York, 1983), pp. 191–263.
24. We thank T. Hoshi for computer programming; S. Germeraad for making tissue cultures; and S. Germeraad, D. O'Dowd, S. Garber, and M. Brainard for comments on the manuscript. Supported by NIH grant NS23294 and a grant from the Searle Scholars Program/Chicago Community Trust (to R.W.A.), an NSF graduate fellowship to C.K.S., and a National Institutes of Health training grant (NS 07158-07) to W.N.Z.

15 December 1986; accepted 17 March 1987

Herbivory in Rocks and the Weathering of a Desert

MOSHE SHACHAK, CLIVE G. JONES,* YIGAL GRANOT

Two species of snail, *Euchondrus albulus* and *Euchondrus desertorum*, eat endolithic lichens growing under the surface of limestone rocks in the Negev Desert, Israel. This unusual type of herbivory has the unexpected and major impact of weathering this rocky desert at a rate of 0.7 to 1.1 metric tons per hectare per year. The biotic weathering contributes to the process of soil formation at a rate that is similar to windborne dust deposition. These findings demonstrate that herbivores can have a significant regulatory impact on ecosystem processes, even in cases where the total amount of primary production consumed is small.

PLANTS HAVE MANY CHARACTERISTICS that make consumption by herbivores difficult. Features of particular importance are low availability of nutrients and water, low digestibility, toughness, and high concentrations of defensive chemicals (*1*). Lichens possess all of the above characteristics, and it has been suggested that lichens should be difficult to consume (*2*). Endolithic lichens that occur under the rock surface should be an even more difficult food to use than epilithic or surface lichens. We report an unusual form of herbivory by two snail species in the Negev Desert. These animals feed on endolithic lichens in the limestone rock. An unexpected consequence of this consumption is that the snails are major agents of rock weathering and soil formation in this desert, despite the relatively small amount of primary production that they consume. The disproportionate impact of the consumption of lichens by snails arises because snails must physically disrupt and ingest the rock substrate in order to consume the lichens. These findings show that herbivores can play an important regulatory role in ecosystem processes, even if they consume small quantities of primary production.

The Negev Desert Highlands, Israel, is a hilly limestone rock desert 500 to 1000 m above sea level with an annual rainfall of 90 mm/year. Seventy percent of the ground area is covered by rocks of various sizes from 10^1 to 10^8 cm^2 (*3*). These rocks are partially covered by epilithic lichens and contain extensive areas of endolithic lichens. Endolithic lichens are the dominant cryptogamic elements in limestone in extreme environments. They consist of a fungal cortex, algal layer, and fungal medulla and occur at depths between 1 and 7 mm in rock (*4*). We observed snails of two species, *Euchondrus albulus* Mousson and *Euchondrus desertorum* Roch, foraging on these rocks. A close examination of foraging areas showed white trails that were the color of raw limestone (limestone without any endolithic lichens); we also saw small piles of feces of the same color. We postulated that snails were feeding on endolithic lichens, which occur within the upper 1 to 3 mm of these rocks (*4*), and were ingesting rock in the process of obtaining food.

We videotaped the foraging behavior of snails on rocks in the laboratory (Fig. 1). Our findings showed that snails moved over the rock surface in what appeared to be a searching behavior, then stopped and changed body orientation so that the shell became almost vertical. They then began a series of short, rapid, side-to-side motions. Snails continued this activity for about 20 minutes per foraging period while moving slowly along the rock, leaving a white mark in the rock. We do not know what cues are used by the snails in selecting a feeding area. One of these white marks was a gouge in the rock surface about 10.3 mm long, 1.1 mm wide, and 0.4 mm deep (Fig. 2). The sides of this gouge clearly showed layers of fungus and algae in the rock, with the white limestone beneath. The depth of the trail appeared to depend on the number of times an old trail had been re-browsed (Fig. 2). It is possible that snails re-browse trails to consume the fungal hyphae that grow into the trail within 48 hours of initial browsing. The radula of both snail species appears to be typical of the family. Cutting teeth have a large cusp with a blunted and curved tip. Injuries and deformities to the teeth are common, presumably as a consequence of feeding. However, there is no evidence of any special radula adaptations in these two species. We presume that teeth are continually regrown to repair those that have been damaged (*5*). We analyzed the calcium content of snail feces and compared the values to those of samples from the top 1 mm of the rock and lichen layer that was removed by the snails. The calcium content was 0.33 mg of Ca^{2+} per milligram of feces and 0.31 mg of Ca^{2+} per milligram of rock and lichen

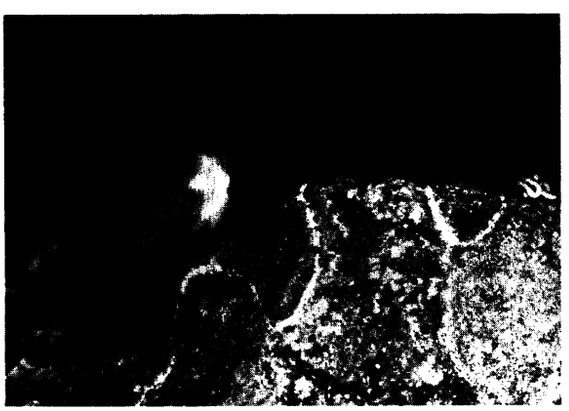

Fig. 1. *Euchondrus desertorum* foraging on a limestone rock containing endolithic lichens. The snail shell is 150 mm long; white feces are on top right-hand side of the rock. The feeding trails scraped in the rock by the snail are the white lines running down the rock between the snail and the feces. [Photograph by Alan Rokach]

M. Shachak, Mitrani Center for Desert Ecology, Jacob Blaustein Institute for Desert Research, Ben-Gurion University of the Negev, Sede Boquer Campus, Israel 84990, and Institute of Ecosystem Studies, New York Botanical Garden, Mary Flagler Cary Arboretum, Millbrook, NY 12545.
C. G. Jones, Institute of Ecosystem Studies, New York Botanical Garden, Mary Flagler Cary Arboretum, Millbrook, NY 12545.
Y. Granot, Mitrani Center for Desert Ecology, Jacob Blaustein Institute for Desert Research, Ben-Gurion University of the Negev, Sede Boquer Campus, Israel 84990.

*To whom correspondence should be addressed.